Super-assembled Biocatalytic Porous Framework Micromotors with Reversible and Sensitive pH-Speed Regulation at Ultralow Physiological H_2O_2 Concentration

Song Gao, Jingwei Hou, Jie Zeng, Joseph J. Richardson, Zi Gu, Xiang Gao, Dongwei Li, Meng Gao, Da-Wei Wang, Pu Chen, Vicki Chen, Kang Liang,* Dongyuan Zhao and Biao Kong**

S. Gao, Dr. Z. Gu, Prof. D.-W. Wang, Prof. V. Chen, Dr. K. Liang

School of Chemical Engineering, The University of New South Wales, NSW 2052, Australia

E-mail: v.chen@unsw.edu.au; kang.liang@unsw.edu.au

Dr. J. Hou

Department of Materials Science and Metallurgy, University of Cambridge, Cambridge CB3 0FS, United Kingdom

J. Zeng, X. Gao, D. Li, M. Gao, Prof. D. Zhao, Prof. B. Kong

Department of Chemistry, Shanghai Key Lab of Molecular Catalysis and Innovative Materials, iChEM, Fudan University, Shanghai, P. R. China

E-mail: bkong@fudan.edu.cn

Dr. J. J. Richardson

Department of Chemical and Biomolecular Engineering, The University of Melbourne, Parkville, Victoria, Australia

X. Gao, D. Li, Dr. K. Liang

National Supercomputer Research Center of Advanced Materials, Advanced Materials Institute, Qilu University of Technology, Shandong Academy of Sciences, Jinan 250014, P. R. China

Prof. P. Chen

Department of Chemical Engineering, University of Waterloo, Waterloo, Ontario, N2L 3G1, Canada

This is the author manuscript accepted for publication and has undergone full peer review but has not been through the copyediting, typesetting, pagination and proofreading process, which may lead to differences between this version and the Version of Record. Please cite this article as doi: 10.1002/adfm.201808900.

Prof. V. Chen

School of Chemical Engineering, University of Queensland, St. Lucia, 4072, Australia

Dr. K. Liang

Graduate School of Biomedical Engineering, The University of New South Wales, Sydney, Australia

Dr. Z. Gu, Dr. K. Liang

Australian Centre for NanoMedicine, The University of New South Wales, NSW 2052, Australia

Keywords: micromotors, biocatalysis, pH-responsive, self-propulsion, metal-organic frameworks

Synthetic nano/micromotors are a burgeoning class of materials with vast promise for applications ranging from environmental remediation to nanomedicine. Motility of these motors is generally controlled by the concentration of accessible fuel, and therefore engineering speed-regulation mechanism, particularly using biological triggers, remains a continuing challenge. Here we demonstrate control over the movement of super-assembled porous framework micromotors (SAFMs) via a reversible, biological-relevant pH-responsive regulatory mechanism. Succinylated β-lactoglobulin and catalase were super-assembled in porous framework particles, where the β-lactoglobulin is permeable at neutral pH. This permeability allows the fuel (H_2O_2) to access catalase leading to autonomous movement of the micromotors. However, at mild acidic pH, succinylated β-lactoglobulin undergoes a reversible gelation process preventing the access of fuel into the micromotors where the catalase resides. To our knowledge this study represents the first example of chemically driven motors with rapid, reversible pH-responsive motility. Furthermore, the porous framework significantly enhances the biocatalytic activity of catalase, allowing ultralow H_2O_2 concentrations to be exploited at physiological conditions. We envision that the simultaneous exploitation of pH and chemical potential of such nanosystems could have potential applications as stimulus-responsive drug delivery vehicles to take the benefit from the complex biological environment.

1. Introduction

Since the pioneering reports in the last decade,[1,2] chemically driven self-propelled nano/micromotors have been receiving increasing attention.[3–8] Inspired by biological molecular motors and self-propelled microorganisms, synthetic motors convert local chemical energy into

kinetic motion, with potential to revolutionize various fields including controlled drug delivery,[9–12] biosensing,[13–15] medical imaging,[16,17] microsurgery,[18–20] and environmental remediation.[21,22] In contrast to biological molecular motors where their speed of movement can be precisely regulated by complex internal and external microenvironments,[23] controlling the movement of synthetic motors is still in its infancy. However, the propulsive speed of synthetic chemically driven motors is generally achieved by catalyzing accessible fuel from the local environment into mechanical energy,[24] which is difficult to tune. Therefore, there is a growing effort to engineer stimulus-responsive speed control mechanisms into synthetic motors for various on-demand applications.[25]

Recently some degree of control over synthetic micromotor speed has been reported either by chemically inhibiting the catalytic system (e.g. by chemically deactivating the active site for a permanent[26] or temporary[27] loss of motion), or by varying external energy input such as heat,[28,29] light,[30–33] or magnetic field.[34] However, the former strategy requires inhibition/reactivation steps *via* the addition/removal of chemicals, while the latter has significant difficulties in reaching remote sites[35] (e.g. deep tissue), and therefore both are not practical for many biomedical applications. As an alternative, exploiting biologically-relevant stimuli, such as pH, redox potential, or by-products of enzymatic activity, as speed control mechanisms for synthetic motors could open up new avenues for next-generation biotechnological applications. Up to now, most reported pH-induced motion manipulation of nano/micromotors requires the sequential addition of acid or base to introduce pH fluctuations.[36–43] However, this is not practical in most real-world scenarios, as it is essentially the same as the aforementioned chemically inhibiting systems. Consequently, autonomous oscillation of environmental pH values combined with pH-regulated motion behavior is highly desired.[25] For instance, the pH across different organs and tissues are highly diverse and precisely regulated in the

human body.[44] In addition, the extracellular pH is different than the pH of many cellular compartments, making pH-stimulus-responsive microsystems an ideal candidate for biomedical applications.[44]

Very recently, metal-organic frameworks (MOFs) have emerged as a new material platform for micromotors.[26,45–47] Constructed from metal ions or clusters bridged by organic ligands, MOFs possess ultraporosity with tunable pore microenvironments.[48,49] More importantly, functional biomolecules can be super-assembled into the porous MOF framework *in situ*, allowing limitless potentials to be exploited.[50–52] Here, we demonstrate the super-assembly of biocatalytic MOF micromotors with an inbuilt biological pH-responsive "on/off" speed regulation mechanism. Succinylated β-lactoglobulin and catalase were super-assembled in MOF particles, where the β-lactoglobulin is permeable at neutral pH. This permeability allows the chemical fuel (H_2O_2) to access catalase leading to autonomous movement of the MOF micromotors. However, at mild acidic pH, succinylated β-lactoglobulin undergoes a reversible gelation process preventing the access of fuel into the micromotors where the catalase resides, hence leading to a reduced motion. The design of biocatalytic MOF micromotors fulfils a number of requirements for the next generation smart micromotor systems, including: 1) exploiting biologically relevant pH variation for tunable autonomous micromotion; 2) ultrahigh loading and embedding of enzymes in the MOF framework that dramatically enhances the biocatalytic H_2O_2 breakdown and in turn the enhanced sensitivity; 3) responding to ultralow, biologically relevant H_2O_2 concentrations (in μm range), dramatically improve the sensitivity and practicability for H_2O_2 fueled micromotors; 4) dual pH and H_2O_2 responsiveness for programmed degradation and release of payload. The super-assembly of

biocatalytic MOF micromotor could have potential applications as stimulus-responsive drug delivery vehicles where the local pH and chemical potential can be simultaneously exploited.

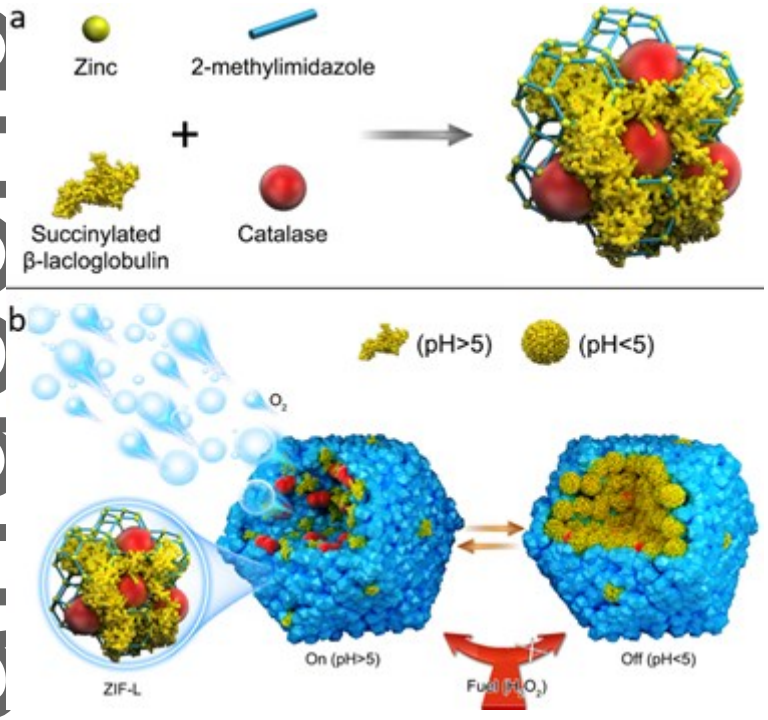

Figure 1. (a) Schematic representation of the assembly of micromotors with pH-responsive on/off motion. Note the relative size between each component is not to scale. (b) Under neutral pH, succinylated β-lactoglobulin remains permeable, allowing fuel to access the micromotor, turning it on; whereas under mild acidic pH, succinylated β-lactoglobulin undergoes a secondary structure transition, thereby turning the micromotors off.

2 Results and Discussion

2.1. Micromotor synthesis and characterization

pH-responsive biocatalytic micromotors were designed and synthesized by super-assembly of catalase and succinylated β-lactoglobulin into zeolitic imidazolate framework-L (ZIF-L) in situ. ZIFs are a subclass family of MOFs, synthesized by copolymerization of either Zn(II) or Co(II) with imidazolate-type links.[53] ZIFs have a high surface area, exceptional chemical and thermal stability, and negligible cytotoxicity.[53,54] In particular, ZIF-L (a type of ZIF) possesses large pore cavities between its unique 2-dimensional (2D) layered structures,[55,56] which could afford more efficient molecular transport properties. While peroxide-powered catalase micromotors have been reported,[57–63] the use of pH-responsive molecules as a gatekeeper to regulate the accessibility of peroxide has not been investigated, and stands as an attractive route for applying micromotors to biomedicine. Succinylated β-lactoglobulin was employed in this work due to its excellent biocompatibility and pronounced pH-induced conformational changes.[64,65] In mild acidic environments this protein undergoes a secondary structure transition, leading to the formation of intermolecular hydrogen-bonding β-sheets.[64] This conformational change is associated with low solubility of the protein resulting in a gel-like structure, which in our system, serves as a valve to reversibly block the access of the peroxide fuel into the micromotors. In contrast, at neutral pH the succinylated β-lactoglobulin transforms to a soluble conformation and becomes permeable, allowing peroxide to regain access to the micromotor (acceleration, **Figure 1**).

Co-entrapment of succinylated β-lactoglobulin and catalase in ZIF-L particles (cat-β@ZIF) was achieved by addition of succinylated β-lactoglobulin and catalase at a 5:1 mass ratio into an aqueous

solution of 2-methylimidazole, followed by the addition of zinc ions. In our previous work, we demonstrated that a range of biomolecules including proteins, enzymes, DNA, polysaccharides, and even living entities can induce the crystallization of a range of MOFs and end up embedded within the porous framework.[50–52,66–69] The addition of succinylated β-lactoglobulin and catalase rapidly induced the formation of particles, as seen by the solution turning turbid within seconds of mixing. The high amount of β-lactoglobulin was used to ensure that enough proteins were present as pH-responsive gatekeepers to control the access of fuel. Scanning and transmission electron microscopy (SEM and TEM, respectively) revealed the formation of particles ~1 μm in diameter with cruciate flower-like morphology (Figure 2a-b), which is similar to pure ZIF-L particles.[55] To assess the final encapsulation efficiency for both proteins, fluorescently labelled succinylated β-lactoglobulin and catalase were employed during the particle synthesis, and the fluorescent intensity was studied and compared against pre-determined calibration curves (Figure S1). Results indicated that *c.a*. 81% β-lactoglobulin and 100% catalase were embedded in ZIF-L particles, corresponding to a final mass ratio of *c.a*. 4 to 1 β-lactoglobulin to catalase. In addition, the cat-β@ZIF-L particles displayed fluorescence from both β-lactoglobulin and catalase in each focal plane under confocal microscopy, further confirming that both proteins were present in the particles (Figure 2c-d). The structure of the recovered cat-β@ZIF particles was assessed by small-angle X-ray scattering (SAXS) and the resulting pattern showed peaks analogous, both in position and relative intensity, to pure ZIF-L crystals (Figure 2e). FTIR measurement performed on the recovered particles showed the presence of characteristic amide bands together with ZIF-L bands, indicating the co-existence of proteins and ZIF-L. In contrast, pure ZIF-L particles post incubated with either or both of the proteins did not show characteristic protein bands after washing (Figure 2f).

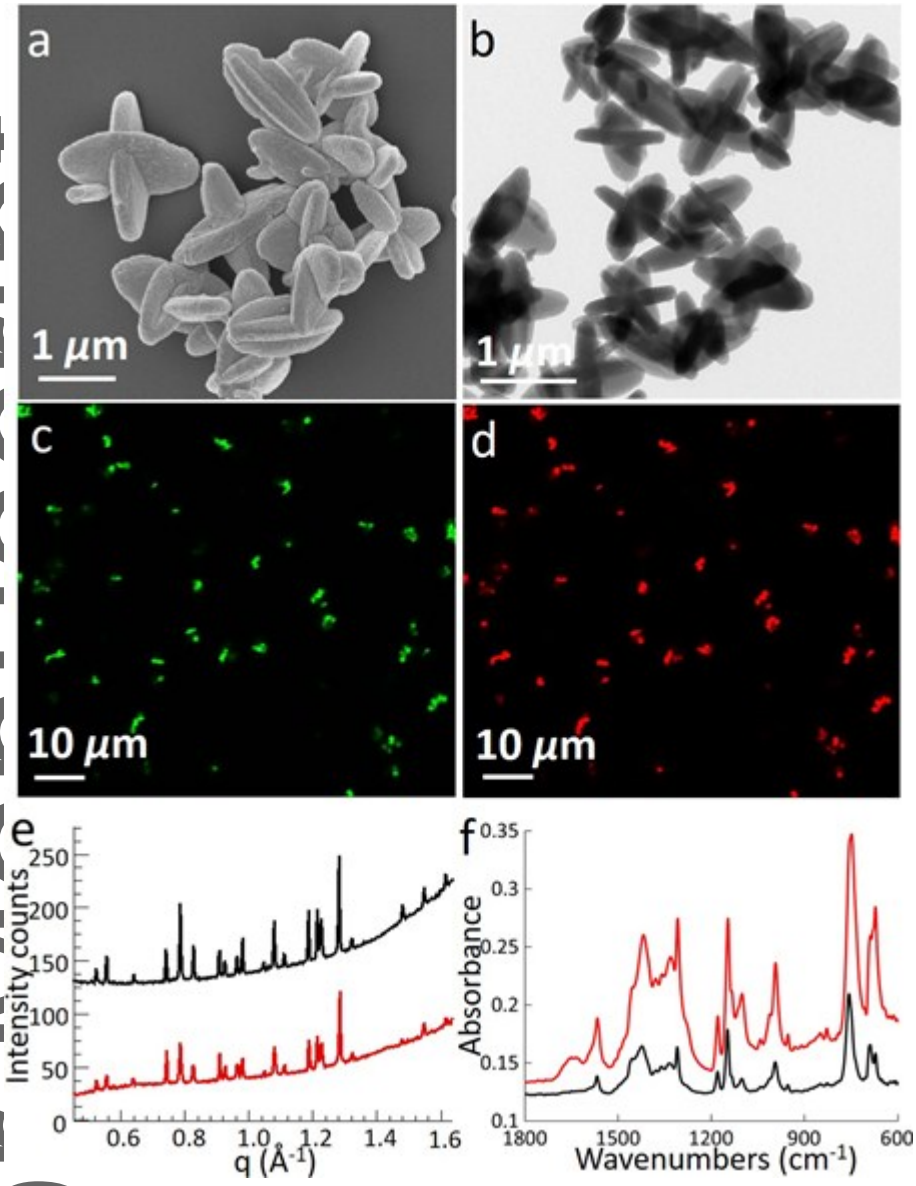

Figure 2. (a) SEM and (b) TEM images of cat-β@ZIF particles. (c-d) Confocal microscopy images of fluorescently labeled cat-β@ZIF particles. Succinylated β-lactoglobulin was labelled with fluorescein isothiocyanate (FITC, green), whereas catalase was labelled with Alexa Fluor 647 (red). (e) Synchrotron SAXS patterns of bare ZIF-L particles (black line) and cat-β@ZIF particles (red line). (f) FT-IR patterns of bare ZIF-L particles (black line) and cat-β@ZIF particles (red line).

2.2. Characterization of biocatalytic efficiency

To determine the catalytic activity of catalase, hydrogen peroxide was introduced to the solution containing free catalase, catalase-loaded ZIF-L particles, and cat-β@ZIF particles, respectively, and the peroxide decomposition was monitored by UV-Vis spectroscopy. There was no apparent difference in peroxide decomposition rate at pH 5 and 7, suggesting that the catalytic activity of both free catalase and super-assembled catalase remained the same across these pH conditions (Figure S2a-b). Furthermore, the super-assembled micromotor particles demonstrated almost 2-fold enhancement of the biocatalytic breakdown (V_0) of H_2O_2 at pH 7 compared to free catalase while pure ZIF-L showed no catalytic activity (Figure S2c). This enhancement can be attributed to the confinement of urease provided by the MOF framework which prevents the enzyme from aggregating in solution,[70,71] while the ultraporous MOF enables efficient molecular diffusion of H_2O_2. It is worth noting that although pure ZIF-L particles are not stable in acidic environments for prolonged periods, the cat-β@ZIF micromotor particles remained stable for at least for 2 h at pH 5 with minimal catalase leaching (Figure S3-S4). This stability could be due to the new coordination bonds formed between the proteins and MOF frameworks, which could contribute to the enhanced stability of the framework, as shown in our previous reports.[50] However, prolonged incubation in acidic environment (> 6 h) eventually led to the complete disassembly of the micromotor particles (Figure S4-S5), highlighting their potential as intracellular delivery vehicles where programmed particle degradation in acidic cellular compartments (e.g. endosomes) could be exploited.

2.3. pH stimulus-responsive behavior

Conventional catalase-based micromotors utilize peroxide to generate oxygen bubbles to propel micromotors, as demonstrated previously.[24] In our study, we hypothesized that the succinylated β-lactoglobulin in the micromotors could serve as a pH-responsive gatekeeper to control the access of fuel to the micromotors. We first employed a small fluorescent molecule, 4',6-diamidino-2-phenylindole (DAPI) to directly visualize whether succinylated β-lactoglobulin can effectively control the access of small molecules via pH change. Succinylated β-lactoglobulin was labelled with FITC for particle tracing purpose. The cat-β@ZIF particles incubated with DAPI at pH 7 showed strong blue emission throughout the particles after washing, indicating that DAPI can freely access the micromotor particles. In contrast, no blue emission was observed after incubating the particles with DAPI at pH 5 (Figure S6). Further confocal fluorescent studies showed that the particles can rapidly switch their permeability 5 s after pH change (Figure S7). These data clearly demonstrate the pH tunable gatekeeping nature of the micromotor particles.

2.4. Characterization of motion behavior

These results motivated us to investigate the autonomous motion of the cat-β@ZIF micromotors in the presence of various hydrogen peroxide concentrations and pH conditions. Nanoparticle-tracking analysis (NTA) was used to record the x and y coordinates of the real-time movement of individual micromotors and provide individual particle-by-particle analysis. This data was further used to plot the average mean square displacement (MSD) curves of particles. When no hydrogen peroxide was

added, the micromotor particles solely displayed typical Brownian motion (Supporting Information video S1), which was similar to bare ZIF-L and single protein (β-lactoglobulin or catalase) loaded ZIF-L particles (Figure 3). To evaluate whether the motion of cat-β@ZIF could be tuned based on controlling the access of H_2O_2 fuel through pH changes, the motion of cat-β@ZIF at pH 5 and pH 7 in the presence of various H_2O_2 concentrations were measured. At pH 7 without H_2O_2, the movement of the nanomotors exhibited a typical "random walk" behavior. However, with the presence of H_2O_2 at pH 7, the travel distance covered by the nanomotors' "walk path" was much greater (Figure 3a, Supporting Information video S2). In addition, cat-β@ZIF particles demonstrated peroxide concentration-dependent movement, with faster movement at higher peroxide concentrations (Figure 3b). This result showed that at pH 7, β-lactoglobulin allowed the H_2O_2 to access the micromotor particles, leading to the more rapid conversion of chemical energy into mechanical work. In contrast, at pH 5, the displacement of cat-β@ZIF particles only showed minimal enhancement in MSD values compared to bare ZIF-L particles in the presence of H_2O_2 (i.e. mainly Brownian motion, see Figure 3b, Supporting Information video S3). These results strongly suggest that β-lactoglobulin can regulate the passage of H_2O_2 into the micromotor particles based on pH variation.

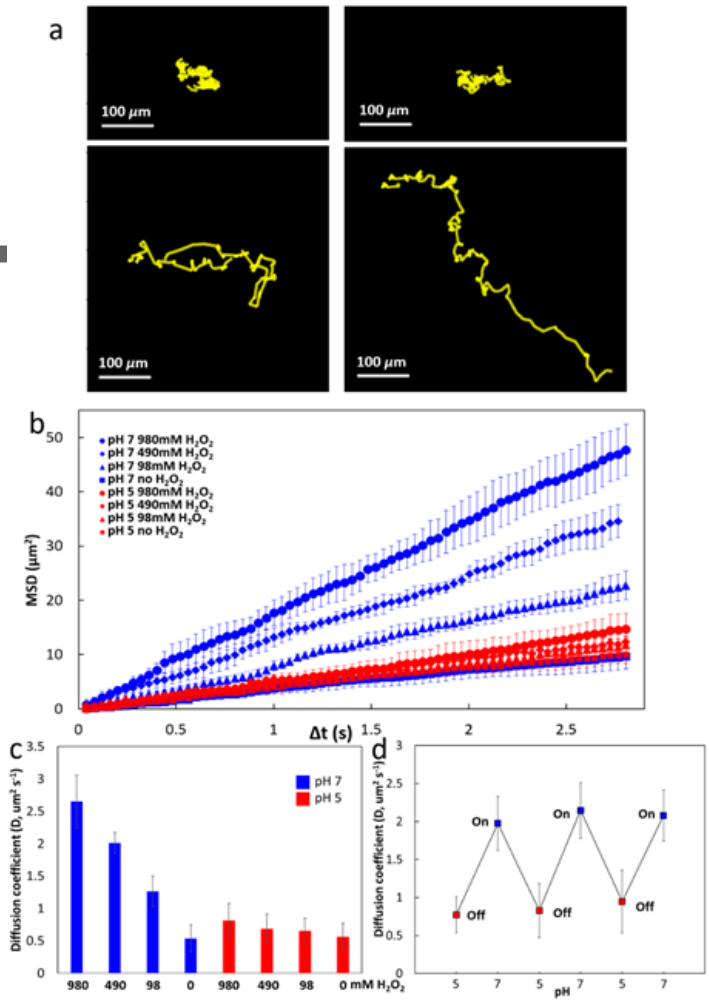

Figure 3. (a) Trajectory tracking of two individual particles at pH 7 without H_2O_2 (top row) and with 490 mM H_2O_2 (bottom row). (b) MSD plot *versus* time interval, analyzed from *x* and *y* coordinate tracking of at least 20 particles at each condition. (c) Diffusion coefficient values calculated from MSD. (d) Three "on/off" motion cycles of cat-β@ZIF micromotors achieved by pH switches (pH 7 = on, pH 5 = off). All error bars indicate the *s.d*. of at least 20 data points.

To gain a better understanding of the system, we calculated the diffusion coefficient of the micromotors under different environments. According to the definition of the diffusion coefficient, D = MSD/i·Δt, where *i* is the dimensional index, and *Δt* is the time interval. For 2-dimensional particle

tracking, *i* is equal to 4.[72] The calculated D for the cat-β@ZIF particles at pH 5 at 98, 490, and 980 mM (0.3, 1.5, and 3%) H_2O_2 was 0.65, 0.68, and 0.81 $\mu m^2/s$ (Figure 3c), respectively, which are slightly higher than to the D values of the micromotor particles without any exposure to H_2O_2 (*i.e.* 0.56 $\mu m^2/s$ at pH 5 and 0.54 $\mu m^2/s$ at pH 7). The slight increase of D value at pH 5 in the presence of H_2O_2 is likely due to the residual catalase activity towards the surface of the particles (Figure 2f). These experimental D values are reasonable when compared to theoretical values calculated from Stokes-Einstein equation for particles of 1 um in diameter, i.e. 0.49 $\mu m^2/s$. In contrast, at pH 7, the diffusion coefficient of the micromotor particles increased significantly with increasing H_2O_2 concentration (i.e. 1.27, 2.01, and 2.65 $\mu m^2/s$ at 98, 490, and 980 mM H_2O_2, respectively, Figure 3c). Owing to the reversible conformational changes of β-lactoglobulin, we next investigated if the micromotor motion could be reversibly switched between the "on" and "off" state. Thus, repeated switching of the buffer containing the micromotor particles between pH 5 and 7 was studied, and at least 20 individual particle displacement information was analyzed by particle tracking for each cycle. As shown in Figure 3d, the repeated switching of the pH values between 5 and 7 resulted in the rapid change of the diffusion coefficient. The switchable motion of cat-β@ZIF particles was fully retained even after six pH sweeps, proving the reversibility and reproducibility of the motion behavior.

2.5. Cellular studies

Peroxide-fueled artificial micromotors hold great potential for biomedical applications. For instance, local tumor sites are known to produce excess levels of H_2O_2 and reduced levels of oxygen (tumor

hypoxia) with slightly lower pH (~pH 7) than normal tissue.[44,73] With the ability to exploit biological H_2O_2 at pH 7 and for the generation of oxygen, these micromotors could have potential as drug delivery vehicles for cancer treatment because of the large porosity of ZIF-L. Therefore, we conducted a proof-of-concept study to demonstrate the cytotoxic effects of drug-loaded cat-β@ZIF micromotor particles to cancer cells (Figure 4a). HeLa cells were cultured at 100 μM H_2O_2 and at pH 7 to simulate the in vivo tumor microenvironment. Cat-β@ZIF particles were loaded with an anticancer drug, doxorubicin (Dox), and then introduced to the cell culture at different quantities. Cell viability was evaluated by a 3-(4,5-dimethylthiazol-2-yl)-2,5-diphenyltetrazolium bromide (MTT) assay after exposure to the micromotor particles for 48 h (Figure S8). Results clearly indicated a dosage-dependent effect, with higher cytotoxicity when more micromotor particles were utilized (Figure 4b and Figure S9). We noted that the cytotoxicity of the micromotor particles arose from a two-stage process. First, the partial release of the drugs from the micromotor particles was achieved as a result of the accelerated micromotion in the tumor microenvironment (in the presence of H_2O_2 at pH 7), followed by cellular uptake and prolonged retention of the particles in acidic compartments (pH 6.3 – 4.7),[74] leading to complete degradation of the particles and drug release. To prove this hypothesis, we further assessed the *in situ* release profile of the micromotor particles using a fluorescent dye (AF488) as a model. At pH 7, a significant enhancement of AF488 release was observed in the presence of H_2O_2 when compared to the negligible release seen in the absence of H_2O_2 fuel, clearly demonstrating that the enhanced movement of cat-β@ZIF micromotors could lead to a more rapid release of cargo (Figure S10-S11). In addition, pre-incubation of Dox-loaded micromotor particles with the cell media in the presence of H_2O_2 showed significant cytotoxic effect to the cells as compared to without the presence of H_2O_2, further proving the hypothesis that partial

drug release was achieved by accelerated micromotion outside the cells. (Figure S12). Next, deconvolution microscopy was employed to study the drug distribution in HeLa cells after incubation with Dox-loaded micromotor particles for 24 h. The Dox showed a diffuse distribution throughout the cells, with a more intense signal strongly colocalized with lysosomal compartments. This suggested that the micromotor particles were successfully internalized by the cells into acidic compartments, where the Dox was released as a result of particle degradation (Figure 4c-e).

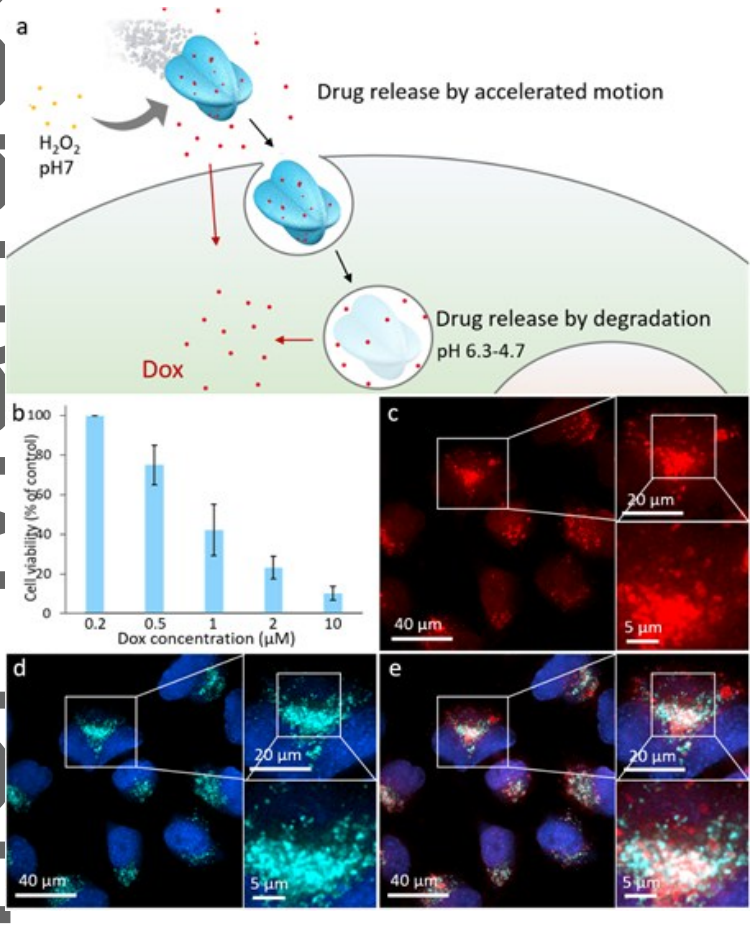

Figure 4. (a) Schematic representation of Dox delivery by cat-β@ZIF prticles. (b) Cell viability of HeLa cells in the presence of Dox-loaded cat-β@ZIF micromotor particles with the Dox concentration calculated based on the total loading amount of Dox in the particles in 1 mL solution. Cell viability was measured by MTT assays after incubation at 37 °C for 48 h. Data show the normalized mean and s.d. of three independent experiments. (c-e) Deconvolution optical microscopy images (maximum

intensity projection) of HeLa cells incubated with Dox-loaded cat-β@ZIF micromotor particles after 48 h. (c) Dox autofluorescence, (d) lysosomes staining using lysosomal-associated membrane protein 1 (LAMP1) antibody (cyan) and cell nuclei (blue), and (e) overlay of (c) and (d).

3. Conclusion

In conclusion, biocatalytic micromotors with autonomous pH-controlled speed "on/off" mechanisms were developed. Succinylated β-lactoglobulin in micromotor particles could act as a biological pH-responsive gatekeeper to regulate the access of H_2O_2 fuel into the micromotor engine. Switching between pH 7 and 5 resulted in sharp micromotor motion response between the "on" and "off" state. Furthermore, proof-of-concept studies demonstrated that the enhanced release of model drugs from the micromotor was achieved under accelerated motion at pH 7 in the presence of H_2O_2, as well as through endocytosis and particle degradation in cellular acidic compartments. Although the research into traditional H_2O_2 fueled micromotors has faced challenges for achieving the required sensitivity at biologically relevant H_2O_2 level, method offered in this work by embedding of catalase into MOFs significantly enhances the catalase activity by 2-fold. This result places the current design as one of the most sensitive H_2O_2-fueled biocatalytic micromotor system suitable for real-life biological applications. In addition, the dual pH and H_2O_2 responsiveness in the micromotor system for programmed degradation and release of payload offer more precise control to deliver drugs to the cells. Nevertheless, further *in vivo* studies are required to validate the full potential and usefulness of the micromotors as stimulus-responsive drug carriers. We envision that this stimulus-responsive strategy using biofriendly proteins is likely to be applied to other types of micromotor systems, allowing the design of the next generation active transport microsystems for drug delivery, biosensing, and bioimaging.

4. Experimental Section

Succinylation of β-lactoglobulin. In a typical experiment, 100 mg of β-lactoglobulin was dissolved in 10 mL of phosphate buffer (50 mM, pH 7.4). Then, 25 mg of succinic anhydride was introduced slowly with stirring at room temperature. The solution was stirred for 1.5 h with the pH maintained between 7.5 and 8.5 by addition of 1 M NaOH. The solution was then transferred to a dialysis tubing (5000-7500 NMWCO) and placed inside a glass beaker containing 1 L of Milli Q water for 24 h at 4 °C (water was changed approx. every 3 h). Finally, the solution was transferred to a round bottom flask and freeze-dried.

Fluorescent labelling of proteins. 35 mg of succinylated of β-lactoglobulin and 0.5 mg of FITC were dissolved in 2.5 mL of phosphate buffer (50 mM, pH 8). The solution was stirred for 1 h at 23 °C. The FITC labelled protein was recovered by pass the solution through a NAP-25 column (GE Healthcare). Fluorescent labelling of catalase was achieved following a similar protocol, instead of FITC, 10 µL of AF647-NHS soultion (1.0 mg/mL in dry DMSO) was added per 35 mg of catalase.

Synthesis of micromotor particles. 100 µL of protein mixture solution, consisting 10 mg of catalase and 2 mg of β-lactoglobulin (2.0 mg) in Milli-Q water, was mixed with 1.0 mL of 2-methylimidazole solution (0.8 M). This was followed by adding 100 µL of zinc nitrate solution (0.5 M) and continually stirred the resultant solution for 30 minutes. The resultant mixture was then centrifuged at 6000 rpm (Eppendorf Centrifuge 5418) for 10 minutes to separate the particles from the supernatant liquid. The particles were then washed with Milli-Q water and centrifuged (3000 rpm) for three

times to remove residual reactants from the particles. The particles were finally resuspended in 1 mL Milli-Q water.

Investigation of particle permeability with 4',6-Diamidino-2-phenylindole dihydrochloride (DAPI). DAPI stock solution was prepared by dissolving 5 mg DAPI in 1 mL Milli-Q water. To investigate the particle permeability, 10 µL DAPI stock solution was introduced to 1 mL buffer solution (pH 5, 50 mM sodium acetate or pH 7, 50 mM Tris) containing the cat-β@ZIF particles under soft agitation. After 10 min, the particles were recovered by centrifugation and washed three times in Milli-Q water and finally resuspended in 1 mL Milli-Q water.

Activity test. The activity of catalase was monitored by UV-Vis spectroscopy at 240 nm as a result of H_2O_2 decomposition. For the activity tests of free catalase, 0.4 mg catalase was dissolved in 2.0 mL of sodium acetate buffer (100 mM) at pH 5 and Tris buffer (50 mM) at pH 7, respectively. To this solution H_2O_2 was introduced to a final concentration of 49 mM. The mixture was transferred to a quartz cuvette and the H_2O_2 concentration was monitored at 240 nm on a UV-Vis spectrophotometer (Cary 300 UV-Vis Spectrophotometer) for 10 min. To test the activity of single-enzyme catalase-loaded particles, equal amount of particle suspension was transferred to 2 mL of sodium acetate buffer (50 mM) at pH 5 and 2 mL of Tris buffer (50 mM) at pH 7 in a quartz cuvette, respectively. H_2O_2 was then introduced to the solution mixture to a final concentration of 49 mM and H_2O_2 concentration was monitored at 240 nm on a UV-Vis spectrophotometer.

Release test. AF488 loaded micromotor particle suspension was combined with 1.0 mL of solution containing 490 mM H_2O_2 at pH 5 (sodium acetate 50 mM) and pH 7 (Tris 50 mM), respectively. At

each time interval, 100 uL of the mixture was removed and centrifuged and the supernatant was assessed on a fluorescence spectrophotometer (Horiba Jobin-Yvon).

Loading of Doxorubicin (Dox). 1 mg of doxorubicin hydrochloride was introduced to 1 mL of micromotor particle solution in water under soft agitation (1.724 mM Dox). After 1 h, the particles were removed and washed three times to recover Dox-loaded particles. Dox loading efficiency was calculated by comparing the Dox concentration in the supernatant after loading against a pre-determined calibration curve. Loading efficiency was ~82%.

Cytotoxicity assay. The 3-(4,5-dimethylthiaol-2-yl)-2,5-diphenyltetrazolium bromide (MTT)-based in vitro cytotoxicity assay was performed according to the method established previously. HeLa or 3T3 cells were seeded on a 96 well plate at a population of 2 × 104 cells per well with (100 μM) and without H_2O_2 in Eagle's MEM with 10% FBS. Various amounts of the Dox-loaded micromotor particles were then introduced to the cell culture, calculated based on the total loading amount of Dox in the particles in 1 mL solution. After incubation for 48 h, 20 μL of MTT (5 mg mL^{-1}) was added to each well. Following 2-h incubation at 37 °C (5% CO2), the MTT product was dissolved in isopropanol and the cell viability was determined from the absorption at 580 nm relative to non-treated cells.

Cell imaging. Deconvolution fluorescence microscopy was performed on a DeltaVision (Applied Precision) microscope with a 60 × 1.42 NA oil objective equipped with a standard FITC/TRITC/CY5 filter set. Images were processed with Imaris (Bitplane) using the maximum intensity projection.

Supporting Information

Supporting Information is available from the Wiley Online Library or from the author.

Acknowledgements

This work was supported by the National Key Research and Development Program of China (2017YFA0206901, 2017YFA0206900), the Australia National Health and Medical Research Council (NHMRC) Career Development Fellowship (APP1163786), the Scientia Fellowship program at UNSW, the Australian Research Council (ARC) Discovery Project (DP190101008), the MCTL Visiting Fellowship Program, the National Natural Science Foundation of China (21705027), the Natural Science Foundation of Shanghai, and the Recruitment Program of Global Experts of China and the Thousand Talent Plan of Shanghai. Part of the experiment was conducted at the Small/wide angle X-ray scattering beamline at the Australian Synchrotron, part of ANSTO.

Received: ((will be filled in by the editorial staff))
Revised: ((will be filled in by the editorial staff))
Published online: ((will be filled in by the editorial staff))

References

[1] W. F. Paxton, K. C. Kistler, C. C. Olmeda, A. Sen, S. K. St. Angelo, Y. Cao, T. E. Mallouk, P. E. Lammert, V. H. Crespi, *J. Am. Chem. Soc.* **2004**, *126*, 13424.

[2] S. Fournier-Bidoz, A. C. Arsenault, I. Manners, G. A. Ozin, *Chem. Commun.* **2005**, *0*, 441.

[3] H. Wang, M. Pumera, *Chem. Rev.* **2015**, *115*, 8704.

[4] M. Guix, C. C. Mayorga-Martinez, A. Merkoçi, *Chem. Rev.* **2014**, *114*, 6285.

[5] F. Wong, K. K. Dey, A. Sen, *Annu. Rev. Mater. Res* **2016**, *46*, 407.

[6] K. Ariga, J. Li, *Adv. Mater.* **2016**, *28*, 987.

[7] K. Ariga, Q. Ji, T. Mori, M. Naito, Y. Yamauchi, H. Abe, J. P. Hill, *Chem. Soc. Rev.* **2013**, *42*,

6322.

[8] K. Ariga, J. Li, J. Fei, Q. Ji, J. P. Hill, *Adv. Mater.* **2016**, *28*, 1251.

[9] W. Gao, B. E. F. de Ávila, L. Zhang, J. Wang, *Adv. Drug Deliv. Rev.* **2017**, DOI: 10.1016/J.ADDR.2017.09.002.

[10] J. Wang, W. Gao, *ACS Nano* **2012**, *6*, 5745.

[11] B. E. F. De Ávila, P. Angsantikul, J. Li, M. Angel Lopez-Ramirez, D. E. Ramírez-Herrera, S. Thamphiwatana, C. Chen, J. Delezuk, R. Samakapiruk, V. Ramez, L. Zhang, J. Wang, *Nat. Commun.* **2017**, *8*, 272.

[12] Y. Tu, F. Peng, P. B. White, D. A. Wilson, *Angew. Chemie Int. Ed.* **2017**, *56*, 7620.

[13] X. Yang, Y. Tang, S. D. Mason, J. Chen, F. Li, *ACS Nano* **2016**, *10*, 2324.

[14] V. V. Singh, K. Kaufmann, B. Esteban-Fernández de Ávila, M. Uygun, J. Wang, *Chem. Commun.* **2016**, *52*, 3360.

[15] O. Ergeneman, G. Chatzipirpiridis, J. Pokki, M. Marin-Suárez, G. A. Sotiriou, S. Medina-Rodriguez, J. F. F. Sanchez, A. Fernandez-Gutiérrez, S. Pane, B. J. Nelson, *IEEE Trans. Biomed. Eng.* **2012**, *59*, 3104.

[16] Z. Wu, B. Esteban-Fernández de Ávila, A. Martín, C. Christianson, W. Gao, S. K. Thamphiwatana, A. Escarpa, Q. He, L. Zhang, J. Wang, *Nanoscale* **2015**, *7*, 13680.

[17] J. Peng, Zhifei Qin, S. Chen, in *2016 IEEE Int. Ultrason. Symp.*, IEEE, **2016**, pp. 1–4.

[18] A. A. Solovev, W. Xi, D. H. Gracias, S. M. Harazim, C. Deneke, S. Sanchez, O. G. Schmidt, *ACS Nano* **2012**, *6*, 1751.

[19] D. Kagan, M. J. Benchimol, J. C. Claussen, E. Chuluun-Erdene, S. Esener, J. Wang, *Angew. Chemie Int. Ed.* **2012**, *51*, 7519.

[20] W. He, J. Frueh, N. Hu, L. Liu, M. Gai, Q. He, *Adv. Sci.* **2016**, *3*, 1600206.

[21] L. Soler, S. Sánchez, *Nanoscale* **2014**, *6*, 7175.

[22] W. Gao, X. Feng, A. Pei, Y. Gu, J. Li, J. Wang, *Nanoscale* **2013**, *5*, 4696.

[23] K. J. Verhey, J. W. Hammond, *Nat. Rev. Mol. Cell Biol.* **2009**, *10*, 765.

[24] X. Ma, A. C. Hortelão, T. Patiño, S. Sánchez, *ACS Nano* **2016**, *10*, 9111.

[25] Y. Tu, F. Peng, D. A. Wilson, *Adv. Mater.* **2017**, *29*, 1701970.

[26] J. Li, X. Yu, M. Xu, W. Liu, E. Sandraz, H. Lan, J. Wang, S. M. Cohen, *J. Am. Chem. Soc.* **2017**, *139*, 611.

[27] X. Ma, X. Wang, K. Hahn, S. Sánchez, *ACS Nano* **2016**, *10*, 3597.

[28] Y. Tu, F. Peng, X. Sui, Y. Men, P. B. White, J. C. M. van Hest, D. A. Wilson, *Nat. Chem.* **2016**, *9*, 480.

[29] V. Magdanz, G. Stoychev, L. Ionov, S. Sanchez, O. G. Schmidt, *Angew. Chemie Int. Ed.* **2014**, *53*, 2673.

[30] S. Palagi, A. G. Mark, S. Y. Reigh, K. Melde, T. Qiu, H. Zeng, C. Parmeggiani, D. Martella, A.

Sanchez-Castillo, N. Kapernaum, F. Giesselmann, D. S. Wiersma, E. Lauga, P. Fischer, *Nat. Mater.* **2016**, *15*, 647.

[31] B. Dai, J. Wang, Z. Xiong, X. Zhan, W. Dai, C.-C. Li, S.-P. Feng, J. Tang, *Nat. Nanotechnol.* **2016**, *11*, 1087.

[32] Z. Wu, X. Lin, Y. Wu, T. Si, J. Sun, Q. He, *ACS Nano* **2014**, *8*, 6097.

[33] R. Dong, Y. Hu, Y. Wu, W. Gao, B. Ren, Q. Wang, Y. Cai, *J. Am. Chem. Soc.* **2017**, *139*, 1722.

[34] A. Zakharchenko, N. Guz, A. M. Laradji, E. Katz, S. Minko, *Nat. Catal.* **2018**, *1*, 73.

[35] Y. Wang, D. S. Kohane, *Nat. Rev. Mater.* **2017**, *2*, 17020.

[36] Y. Tu, F. Peng, A. A. M. André, Y. Men, M. Srinivas, D. A. Wilson, *ACS Nano* **2017**, *11*, 1957.

[37] Y. Dong, M. Liu, H. Zhang, B. Dong, *Nanoscale* **2016**, *8*, 8378.

[38] M. Xiao, M. Cheng, Y. Zhang, F. Shi, *Small* **2013**, *9*, 2509.

[39] M. Xiao, X. Guo, M. Cheng, G. Ju, Y. Zhang, F. Shi, *Small* **2014**, *10*, 859.

[40] M. Guix, A. K. Meyer, B. Koch, O. G. Schmidt, *Sci. Rep.* **2016**, *6*, 21701.

[41] W. Gao, A. Uygun, J. Wang, *J. Am. Chem. Soc.* **2012**, *134*, 897.

[42] J. Li, S. Thamphiwatana, W. Liu, B. Esteban-Fernández de Ávila, P. Angsantikul, E. Sandraz, J. Wang, T. Xu, F. Soto, V. Ramez, X. Wang, W. Gao, L. Zhang, J. Wang, *ACS Nano* **2016**, *10*, 9536.

[43] W. Gao, R. Dong, S. Thamphiwatana, J. Li, W. Gao, L. Zhang, J. Wang, *ACS Nano* **2015**, *9*, 117.

[44] B. A. Webb, M. Chimenti, M. P. Jacobson, D. L. Barber, *Nat. Rev. Cancer* **2011**, *11*, 671.

[45] Y. Ikezoe, G. Washino, T. Uemura, S. Kitagawa, H. Matsui, *Nat. Mater.* **2012**, *11*, 1081.

[46] Y. Ikezoe, J. Fang, T. L. Wasik, T. Uemura, Y. Zheng, S. Kitagawa, H. Matsui, *Adv. Mater.* **2015**, *27*, 288.

[47] T. T. Y. Tan, J. T. M. Cham, M. R. Reithofer, T. S. A. Hor, J. M. Chin, *Chem. Commun. (Camb).* **2014**, *50*, 15175.

[48] O. M. Yaghi, M. O'Keeffe, N. W. Ockwig, H. K. Chae, M. Eddaoudi, J. Kim, *Nature* **2003**, *423*, 705.

[49] H.-C. J. Zhou, S. Kitagawa, *Chem. Soc. Rev.* **2014**, *43*, 5415.

[50] K. Liang, R. Ricco, C. M. Doherty, M. J. Styles, S. Bell, N. Kirby, S. Mudie, D. Haylock, A. J. Hill, C. J. Doonan, P. Falcaro, *Nat. Commun.* **2015**, *6*, 7240.

[51] K. Liang, R. Wang, M. Boutter, C. M. Doherty, X. Mulet, J. J. Richardson, *Chem. Commun.* **2017**, *53*, 1249.

[52] Y. Chu, J. Hou, C. Boyer, J. J. Richardson, K. Liang, J. Xu, *Appl. Mater. Today* **2018**, *10*, 93.

[53] K. S. Park, Z. Ni, A. P. Côté, J. Y. Choi, R. Huang, F. J. Uribe-Romo, H. K. Chae, M. O'Keeffe, O. M. Yaghi, *Proc. Natl. Acad. Sci. U. S. A.* **2006**, *103*, 10186.

[54] X.-C. Huang, Y.-Y. Lin, J.-P. Zhang, X.-M. Chen, *Angew. Chem. Int. Ed. Engl.* **2006**, *45*, 1557.

[55] J. Cui, Y. Feng, T. Lin, Z. Tan, C. Zhong, S. Jia, *ACS Appl. Mater. Interfaces* **2017**, *9*, 10587.

[56] Z. Zhong, J. Yao, R. Chen, Z. Low, M. He, J. Z. Liu, H. Wang, *J. Mater. Chem. A* **2015**, *3*, 15715.

[57] Y. Wu, X. Lin, Z. Wu, H. Möhwald, Q. He, *ACS Appl. Mater. Interfaces* **2014**, *6*, 10476.

[58] X. Ma, S. Sanchez, *Chem. Commun.* **2015**, *51*, 5467.

[59] S. Sanchez, A. A. Solovev, Y. Mei, O. G. Schmidt, *J. Am. Chem. Soc.* **2010**, *132*, 13144.

[60] R. Golestanian, T. B. Liverpool, A. Ajdari, *Phys. Rev. Lett.* **2005**, *94*, 220801.

[61] X. Ma, X. Wang, K. Hahn, S. Sánchez, *ACS Nano* **2016**, *10*, 3597.

[62] P. Schattling, B. Thingholm, B. Städler, *Chem. Mater.* **2015**, *27*, 7412.

[63] K. K. Dey, X. Zhao, B. M. Tansi, W. J. Méndez-Ortiz, U. M. Córdova-Figueroa, R. Golestanian, A. Sen, *Nano Lett.* **2015**, *15*, 8311.

[64] C. Bhattacharjee, S. Saha, A. Biswas, M. Kundu, L. Ghosh, K. P. Das, *Protein J.* **2005**, *24*, 27.

[65] R. Guillet-Nicolas, A. Popat, J.-L. Bridot, G. Monteith, S. Z. Qiao, F. Kleitz, *Angew. Chemie Int. Ed.* **2013**, *52*, 2318.

[66] K. Liang, J. J. Richardson, J. Cui, F. Caruso, C. J. Doonan, P. Falcaro, *Adv. Mater.* **2016**, *28*, 7910.

[67] J. J. Richardson, K. Liang, *Small* **2018**, *14*, 1702958.

[68] B. Kong, L. Zu, C. Peng, Y. Zhang, W. Zhang, J. Tang, C. Selomulya, L. Zhang, H. Chen, Y. Wang, Y. Liu, H. He, J. Wei, X. Lin, W. Luo, J. Yang, Z. Zhao, Y. Liu, J. Yang, D. Zhao, *J. Am. Chem. Soc.* **2016**, *138*, 16533.

[69] B. Kong, J. Tang, Y. Zhang, T. Jiang, X. Gong, C. Peng, J. Wei, J. Yang, Y. Wang, X. Wang, G. Zheng, C. Selomulya, D. Zhao, *Nat. Chem.* **2016**, *8*, 171.

[70] A. S. Vikulina, N. A. Feoktistova, N. G. Balabushevich, A. G. Skirtach, D. Volodkin, *Phys. Chem. Chem. Phys* **2018**, *20*, 8822.

[71] K. Liang, C. J. Coghlan, S. G. Bell, C. Doonan, P. Falcaro, *Chem. Commun.* **2016**, *52*, 473.

[72] X. Ma, K. Hahn, S. Sanchez, *J. Am. Chem. Soc.* **2015**, *137*, 4976.

[73] H. Sies, *Redox Biol.* **2017**, *11*, 613.

[74] J. R. Casey, S. Grinstein, J. Orlowski, *Nat. Rev. Mol. Cell Biol.* **2010**, *11*, 50.

Biocatalytic super-assembled metal-organic framework micromotors with a built-in pH-controlled "on/off" switch is synthesized. Micromotor motion is precisely tuned by the pH-induced reversible protein conformational change within the frameworks that act as a gate keeper to control the access of chemical fuels. Such nanosystem could have potential applications as smart drug delivery vehicles where diffusive transport can be accelerated with triggered micromotion.

Keyword micromotors, biocatalysis, pH-responsive, self-propulsion, metal-organic frameworks

S. Gao, J. Hou, J. Zeng, J. J. Richardson, Z. Gu, X. Gao, D. Li, M. Gao, D.-W. Wang, P. Chen, V. Chen,* K. Liang,* D. Zhao, B. Kong*

Super-assembled Biocatalytic Porous Framework Micromotors with Reversible and Sensitive pH-Speed Regulation at Ultralow Physiological H_2O_2 Concentration

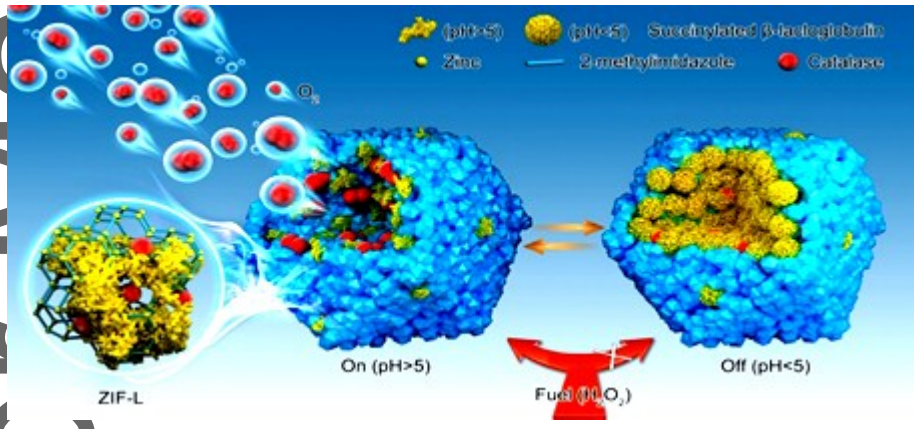

Author/s:
Gao, S;Hou, J;Zeng, J;Richardson, JJ;Gu, Z;Gao, X;Li, D;Gao, M;Wang, D-W;Chen, P;Chen, V;Liang, K;Zhao, D;Kong, B

Title:
Superassembled Biocatalytic Porous Framework Micromotors with Reversible and Sensitive pH-Speed Regulation at Ultralow Physiological H2O2 Concentration

Date:
2019-05-02

Citation:
Gao, S., Hou, J., Zeng, J., Richardson, J. J., Gu, Z., Gao, X., Li, D., Gao, M., Wang, D. - W., Chen, P., Chen, V., Liang, K., Zhao, D. & Kong, B. (2019). Superassembled Biocatalytic Porous Framework Micromotors with Reversible and Sensitive pH-Speed Regulation at Ultralow Physiological H2O2 Concentration. ADVANCED FUNCTIONAL MATERIALS, 29 (18), https://doi.org/10.1002/adfm.201808900.